Title

Trafficking and surface expression of hyperpolarization-activated cyclic nucleotide-gated channels in hippocampal neurons.

Journal

The Journal of biological chemistry, 285(19)

ISSN

0021-9258

Authors

Noam, Yoav
Zha, Qinqin
Phan, Lise
et al.

Publication Date

2010-05-01

DOI

10.1074/jbc.m109.070391

THE JOURNAL OF BIOLOGICAL CHEMISTRY VOL. 285, NO. 19, pp. 14724–14736, May 7, 2010

Trafficking and Surface Expression of Hyperpolarization-activated Cyclic Nucleotide-gated Channels in Hippocampal Neurons*[S]

Received for publication, September 25, 2009, and in revised form, March 4, 2010 Published, JBC Papers in Press, March 9, 2010, DOI 10.1074/jbc.M109.070391

Yoav Noam[‡§], Qinqin Zha[‡], Lise Phan[‡], Rui-Lin Wu[‡], Dane M. Chetkovich[¶], Wytse J. Wadman[§], and Tallie Z. Baram[‡‖1]**

*From the Departments of [‡]Pediatrics, [‖]Anatomy and Neurobiology, and **Neurology, University of California, Irvine, California 92697, the [¶]Department of Neurology and Clinical Neurosciences, Northwestern University, Chicago, Illinois 60611, and the [§]Swammerdam Institute for Life Sciences-Center for NeuroScience, University of Amsterdam, 1098 XH Amsterdam, The Netherlands*

Hyperpolarization-activated cyclic nucleotide-gated (HCN) channels mediate the hyperpolarization-activated current I_h and thus play important roles in the regulation of brain excitability. The subcellular distribution pattern of the HCN channels influences the effects that they exert on the properties and activity of neurons. However, little is known about the mechanisms that control HCN channel trafficking to subcellular compartments or that regulate their surface expression. Here we studied the dynamics of HCN channel trafficking in hippocampal neurons using dissociated cultures coupled with time lapse imaging of fluorophore-fused HCN channels. HCN1-green fluorescence protein (HCN1-GFP) channels resided in vesicle-like organelles that moved in distinct patterns along neuronal dendrites, and these properties were isoform-specific. HCN1 trafficking required intact actin and tubulin and was rapidly inhibited by activation of either NMDA or AMPA-type ionotropic glutamate receptors in a calcium-dependent manner. Glutamate-induced inhibition of the movement of HCN1-GFP-expressing puncta was associated with increased surface expression of both native and transfected HCN1 channels, and this surface expression was accompanied by augmented I_h. Taken together, the results reveal the highly dynamic nature of HCN1 channel trafficking in hippocampal neurons and provide a novel potential mechanism for rapid regulation of I_h, and hence of neuronal properties, via alterations of HCN1 trafficking and surface expression.

The ion channel repertoire of neurons contributes critically to the regulation of neuronal activity. The response of a neuron to an incoming input depends (among other factors) on the molecular composition of its ion channels, their relative abundance, their subcellular location, and the fine tuning of their biophysical properties (1, 2). Mechanisms that control the function, expression levels, and/or subcellular localization of ion channels can influence neuronal function in many ways and at different time scales (1, 2). During the past decade, dynamic regulations of ion channel trafficking and surface expression have emerged as pivotal mechanisms in many forms of neuronal plasticity. However, whereas substantial advances have been made in uncovering the cellular dynamics of *synaptic* ion channel trafficking (3), less is known about the transport of *extrasynaptic* dendritic channels that contribute to intrinsic excitability.

Hyperpolarization-activated cyclic nucleotide-gated (HCN)[2] channels are a family of voltage-gated ion channels that mediate a non-selective cationic current named I_h. Unlike other voltage-gated ion channels, members of the HCN family are activated upon hyperpolarization of the cell membrane, and this unusual feature endows them with unique and versatile roles in the regulation of neuronal excitability (4). The subcellular distribution of HCN channels varies in different cell types and brain regions and is important for determining the effects that these channels exert on neuronal excitability (5). For example, in CA1 hippocampal pyramidal neurons, HCN1 channels are concentrated in the apical dendrites, and channel density is much higher in the distal compared with the proximal dendritic span (6). This gradient has been shown to contribute to normalizing dendritic inputs arriving at different locations along the dendrite (7). In another region of the hippocampal formation, the entorhinal cortex, HCN1 channels are enriched in axon terminals during development, and this localization is developmentally regulated, diminishing in the adult (8). Interestingly, patterns of distribution of HCN1 channels have been recently shown to depend on neuronal network activity. Elimination of synchronized neuronal input to the distal dendrites of CA1 pyramidal neurons abolished the gradient of HCN1 channel distribution (9), and manipulation of activity levels modified the axonal presynaptic expression of HCN1 in entorhinal cortex neurons (8). These forms of activity-dependent regulation

* This work was supported, in whole or in part, by National Institutes of Health Grants R37 NS35439 (to T. Z. B. and Y. N.) and K02NS05595 and R01NS059934 (to D. M. C.). This work was also supported by Dutch Epilepsy Fund Grant NEF 08-02 (to W. J. W. and Y. N.).

[S] The on-line version of this article (available at http://www.jbc.org) contains supplemental Figs. 1–4 and Movies S1–S5.

[1] To whom correspondence should be addressed: Pediatrics and Anatomy/Neurobiology, University of California, Irvine, ZOT 4475, Irvine, CA 92697-4475. Tel.: 949-824-1063; Fax: 949-824-1106; E-mail: tallie@uci.edu.

[2] The abbreviations used are: HCN, hyperpolarization-activated cyclic nucleotide-gated cation; GFP, green fluorescent protein; NMDA, *N*-methyl-D-aspartic acid; AMPA, α-amino-3-hydroxyl-5-methyl-4-isoxazole-propionate; DIV, day(s) *in vitro*; HA, hemagglutinin; MAP2, microtobule-associated protein 2; GAD-65, glutamic acid decarboxylase 65; P*n*, postnatal day *n*.

of HCN channel distribution take place at time scales of days. However, it is unknown if HCN channel transport to subcellular compartments and modulation of surface expression of the channels may take place more rapidly, at the time scale of minutes. These alterations in channel distribution, in turn, might provide the basis for rapid changes in I_h that contribute to types of neuronal plasticity that take place within minutes (10, 11).

In this study, we sought to examine directly the dynamics of HCN channel trafficking and surface expression and their rapid regulation by neuronal activity. Although heterologous expression systems provide valuable information regarding basic cellular processes, the complexity of neuronal systems imposed by the polarized morphology of neurons and their unique electrical activity cannot be reproduced in heterologous models. Therefore, we expressed GFP-fused HCN channels in cultured hippocampal neurons and employed time lapse imaging to study the kinetics of the trafficking of these channels. We found that HCN1-GFP channel proteins were expressed on the cell membrane of hippocampal neurons, where they exhibited biophysical properties similar to wild-type channels. Time-lapse live imaging revealed that HCN1-GFP channel protein was present in vesicle-like organelles that moved bidirectionally along dendrites, and these distribution patterns and mobility differed from those of the HCN2 channel isoform. Trafficking of HCN1-GFP puncta required actin and microtubules and was drastically inhibited by exposure to the excitatory amino acid glutamate, via a process that involved calcium and both NMDA- and AMPA-type glutamate receptors. The rapid glutamate-induced arrest of HCN1 channel movement was associated with a reversible increase of HCN1 channel surface expression and with augmented I_h. Taken together, these findings demonstrate the dynamic nature of HCN1 channel trafficking and suggest a novel mechanism by which neuronal activity can up-regulate I_h within minutes via alterations of HCN1 channel trafficking and surface expression.

EXPERIMENTAL PROCEDURES

Hippocampal Cell Culture

Dissociated hippocampal primary cultures were prepared from postnatal day 0 (P0) Sprague-Dawley rats. Hippocampi were quickly dissected, removed from adherent meninges, and incubated for 30 min in buffered salt solution containing 10 units/ml papain (Worthington). After removal of the papain, cells were mechanically triturated and plated at a density of 400–600 cells/mm^2 on 12-mm coverslips that were precoated with poly-D-lysine (Sigma). Cultures were initially maintained in Neurobasal Medium with B-27 supplement (Invitrogen) at 36 °C and 5% CO_2. 3–4 h after plating, half of the culture medium was replaced with a Neurobasal Medium/B-27-based medium that was preconditioned for 24 h by 1–2-week old non-neuronal cell culture prepared from P3-P4 rat cortices. Cultures were subsequently refreshed every 3–4 days with the conditioned medium. On the third day *in vitro* (DIV), 1 μM cytosine-arabinoside (Sigma) was added to the culture medium to inhibit glial proliferation. All experiments complied with National Institutes of Health (Bethesda, MD) and University of California, Irvine (Irvine, CA) animal care regulations.

Plasmid DNA Constructs

cDNA constructs containing the GFP sequence in the C terminus of the mouse HCN1 cDNA (inserted between amino acid residues 885 and 886) or the hemagglutinin (HA) tag at the HCN1 extracellular domain between transmembrane domains S3 and S4 (residues 231–232) were generated as described previously (12). The N terminus GFP-conjugated mHCN1 (HCN1-GFPn) and mHCN2 (HCN2-GFP) constructs were a gift from Dr. Santoro (Columbia University); previous studies found that the two constructs yielded functional I_h with biophysical properties typical for the respective isoform expressed in heterologous systems (13). mCherry-HCN1 was created by inserting the cDNA encoding mCherry from pRSET-B-mCherry (generously provided by Dr. Roger Tsien, University of California, San Diego) instead of the GFP in the AgeI/XhoI site of the HCN1-GFPn construct.

Neuronal Transfection of Plasmid DNA

Primary neuronal cultures were transfected with plasmid DNA constructs on DIV 7–10, using the Lipofectamine 2000 method (Invitrogen). Transfection mixtures that included 100 μl of Opti-MEM I (Invitrogen), 2 μg of Lipofectamine, and 0.5–1 μg of plasmid DNA were incubated at room temperature for 20 min and then added to each coverslip. To reduce potential toxicity of the lipocationic transfection reagent, the transfection mixture was removed entirely at 1.5–2 h post-transfection, and cultures were refreshed with Neurobasal Medium plus B-27 medium that was CO_2- and temperature-equilibrated prior to transfection, as described in a previously published protocol (14). The membrane capacitance of transfected neurons as measured by whole-cell voltage clamp recording (32.2 $\pm$ 2.5 picofarad; $n = 19$) was not different from that of age-matched, naive, non-transfected neurons (33.8 $\pm$ 6.4 picofarads; $n = 9$; $p > 0.05$) or of non-transfected neurons that were exposed to the Lipofectamine 2000 reagent for a similar duration of time (33.0 $\pm$ 5.0 picofarad; $n = 6$; $p > 0.05$). GFP signal was detected in transfected neurons as early as 6 h after transfection, was stable during the 24–48 h time window, and persisted for a minimum of 72 h post-transfection. Therefore, all experiments were performed 24–48 h post-transfection. Pilot experiments demonstrated that transfection efficiency was 2–6% when using 0.5–1 μg of plasmid DNA per coverslip. Increasing DNA concentrations did not result in higher transfection efficiency, and reducing DNA amounts below 0.5 μg resulted in a significant reduction in transfection efficiency ($<$1%).

Disruption of Microtubules and Actin

To test the involvement of cytoskeletal elements in HCN trafficking, jasplakinolide (Invitrogen) or nocodazole (Sigma) was freshly diluted from frozen stock aliquots to a final concentration of 0.5 and 10 μM, respectively, in 0.06% DMSO (vehicle control).

Time Lapse Live Imaging and Analysis

Live cultured neurons expressing HCN1-GFP or HCN2-GFP were either kept in bath solution (see below) or subjected to

increased synaptic excitation via the application of glutamate (10 μM for 10 min). In experiments testing the involvement of ionotropic glutamate receptors, the specific NMDA receptor blocker amino-5-phosphonovaleric acid (100 μM; Sigma) or the AMPA receptor blocker 6-cyano-7-nitroquinoxaline-2,3-dione (50 μM; Sigma) was added to the bath solution 10 min prior to imaging. Neurons were imaged using a Nikon TE-2000U inverted microscope, using a ×40 objective (numerical aperture 0.60). Coverslips were placed in a bath chamber containing HEPES-buffered bath solution: 110 mM NaCl, 5 mM KCl, 1.8 mM $CaCl_2$, 1.3 mM $MgCl_2$, 10 mM D-glucose, 10 mM HEPES, pH 7.40. The bath solution was adjusted with sucrose to 290–300 mosM and kept at 34–36 °C throughout the experiment. In experiments testing the role of extracellular calcium, calcium was excluded from the HEPES-buffered solution described above, and 5 mM EGTA was added. Cells with a healthy appearance and relatively low HCN1-GFP or HCN2-GFP expression levels were selected for imaging and analysis. Only one cell was chosen from each coverslip, to minimize interdependence of observations. In most time lapse sessions, 39 images were acquired at intervals of 5 s (total time, 190 s), with an exposure time of 500 ms/image. In experiments involving more than two imaging sessions (*e.g.* studies of the reversibility of the glutamate effect on HCN1-GFP trafficking), only 20 or 25 images were taken per session, to limit photobleaching. Images were captured using a CCD monochrome 12-bit camera (Retiga 2000R; Qimaging), acquired with NIS-Elements-D software (Nikon), and colorized for presentation.

For the analysis of puncta mobility, a custom-written program in MATLAB (Mathworks) was used, which enabled manual tracking of single puncta and storage of relevant information for each punctum (such as the kinetic properties of the movement, location, size, and light intensity). To be classified as "mobile," puncta had to move >0.36 μm (equivalent to >2 pixels) at least twice during the sampling period. Analyses of velocity, pause time, and directionality (Figs. 3 and 4) were based on mobile puncta only, which comprised 27.7% of the total HCN1-GFP puncta population (based on >1500 puncta from 11 neurons) and 6.1% of HCN2-GFP (based on 498 puncta from 6 neurons; see Fig. 4). The directionality index presented in Fig. 3*F* was calculated for each punctum using the following formula,

$$\text{Directionality} = \frac{\sum D_{\text{distal}} - \sum D_{\text{proximal}}}{\sum D_{\text{total}}} \qquad \text{(Eq. 1)}$$

where D_{distal} represents the distance traveled by a punctum away from the soma during the sampling period, D_{proximal} represents the distance traveled toward the soma, and D_{total} represents the total distance traveled in both directions. If a punctum moved exactly the same distance toward and away from the soma, its directionality index would be 0 (representing a bidirectional punctum), whereas a movement solely in one direction would yield a value of −1 for a pure centripetal movement and +1 for a pure centrifugal movement. The *absolute* value of directionality (Fig. 3*G*) represents the degree to which a puncta was uni- or bidirectional.

The time course of the glutamate-induced arrest shown in Fig. 6*B* was calculated by quantifying the fraction of mobile puncta (normalized to the total puncta population for each cell) throughout the sampling period and then binning it into 30-s time frames (the first 10 s of the 190-s imaging period were not included in the analysis to enable equally binned periods of 30 s). Pooled, quantitative analysis of HCN1-GFP mobility under different conditions (Fig. 6*E*) was performed as follows. The fraction of mobile puncta was calculated for each cell during the 3-min imaging epoch prior to treatment and during the 3-min epoch starting 7 min following treatment. The post-treatment value was then expressed as a percentage of the pre-treatment value for each cell. Statistical significance was determined using a paired *t* test (two-tailed). Kymographs were generated in ImageJ (National Institutes of Health), using the "multiple kymograph" plug-in (J. Rietdorf and A. Seitz). All analyses were performed without knowledge of the experimental condition.

Immunocytochemisty

Fixed Cells—Neurons were fixed in phosphate-buffered saline with 4% paraformaldehyde for 20 min on ice, permeabilized with 0.1% Triton X-100, and blocked with 5% normal goat serum and 1% bovine serum albumin. Antibodies used included rabbit anti-HCN1 (1:4000; Chemicon; Lot number 0605029427), guinea pig anti-HCN1 (1:4000) (9), or monoclonal mouse anti-HCN1 (1:4000; NeuroMab; clone N70/2); mouse anti-GAD-65 (1:1000; Roche Applied Science); mouse anti-MAP-2 (1:16000; Sigma); and monoclonal mouse anti-α-tubulin (1:1000 Sigma). Immunolabeling of endogenous HCN1 (Fig. 3*A*) was accomplished using tyramide signal amplification according to the manufacturer's instructions (PerkinElmer Life Sciences). Labeling of F-actin was accomplished by incubating neurons with 165 nM Alexa-Fluor 568-conjugated phalloidin (Invitrogen) for 30 min, followed by rigorous washes.

Differential Labeling of Internal and Surface HCN1 Channel Protein—Labeling of surface HA-HCN1 channels was performed on live neurons without detergents (to avoid cell permeabilization). First, HA-HCN1-transfected cultures were incubated with either glutamate or bath solution (vehicle) at 36 °C in a manner similar to that described for the time lapse imaging experiments. After a 10-min incubation, cultures were transferred to 4 °C (to arrest trafficking processes) and incubated with mouse monoclonal HA antibody (1:100; Covance; clone 16B12) for 40 min, followed by a 15-min incubation with Alexa-488-conjugated anti-mouse IgG (1:600; Invitrogen). Cells were then fixed, permeabilized, and blocked, followed by overnight incubation with monoclonal rat anti-HA (1:500; Roche Applied Science; clone 3F10) at 4 °C, to label the remaining (intracellular) HA-HCN1 channels. Antibody displacement was unlikely in this experimental set-up because fixation of the cells *after* surface labeling with the first primary antibody stabilized the antibody-antigen complex. Images were captured using a laser-scanning confocal microscope (Olympus IX-70), with a LaserSharp 2000 (Bio-Rad) acquisition software. Images were acquired with a ×60 objective (numerical aperture 1.40), except for the image in Fig. 1*D*, which was obtained with a ×20 objective. Imaging of surface HA-HCN1 channels was per-

formed with equal exposure parameters for all neurons of the same experiment, and neurons from three independent experiments (2–4 coverslips/condition/experiment) were imaged and analyzed. Three apical dendritic segments, located 50–200 μm away from the soma, were selected per neuron. For each dendritic segment, background intensity levels were measured, and only pixels that had intensity values significantly higher ($p < 0.05$) than background were included in the analyses. Using the histogram function in the ImageJ software (National Institutes of Health), pixels with significant signal intensity in the green or red color channels (representing surface and intracellular HA-HCN1 channels, respectively) were counted, and a surface/total ratio was derived. In total, 33 dendritic segments from 11 cells were analyzed per condition.

Electrophysiology

I_h was recorded from visually identified pyramidal-like neurons in dissociated hippocampal cell cultures using standard whole-cell patch clamp techniques. The bath solution contained 125 mM NaCl, 4 mM KCl, 1.25 mM NaH_2PO_4, 25 mM $NaHCO_3$, 2.0 mM $CaCl_2$, 1.0 mM $MgCl_2$, and 20 mM dextrose. The bath solution was bubbled with 95% O_2, 5% CO_2 and continuously superfused at a rate of 1–1.5 ml/min. In initial experiments aimed to characterize I_h in cultured hippocampal neurons, $BaCl_2$ (0.5 mM) was added to block inward rectifier potassium currents ($I_{k(ir)}$), and $NiCl_2$ (0.1 mM) was added to block low threshold calcium currents. Tetrodotoxin (0.5–1 mM) was added to suppress action potentials, and amino-5-phosphonovaleric acid (20 μM), 6-cyano-7-nitroquinoxaline-2,3-dione (10 μM), and bicuculline (5 μM) were added to block spontaneous synaptic events. When modulation of I_h by activity was examined, none of the blockers mentioned above were added. Recording electrodes were pulled from borosilicate glass capillaries (Sutter Instruments). The pipette was filled with 120 mM potassium gluconate, 20 mM KCl, 2 mM $MgCl_2$, 0.5 mM $CaCl_2$, 5 mM EGTA, 20 mM HEPES, 4.0 mM Na_2-ATP, 0.3 mM Na_2-GTP, adjusted to pH 7.3 with Tris-Cl and adjusted to 295 mosM. Pipette resistance as measured in the bath solution was 4–6 megaohms. Data were collected using an Axopatch 700A amplifier, a Digidata 1322A 16-bit data acquisition system, and pClamp software version 9.2 (Molecular Devices). Voltage and current traces were filtered at 1 and 5 kHz and digitized at 10 and 20 kHz, respectively. Measurements of membrane input resistance (*Rm*) and capacitance (*Cm*) were performed by applying a 10-mV test pulse from a holding potential of −70 to −60 mV for a duration of 10 ms. Calculation of final *Cm* and *Rm* values followed the method first described by Lindau and Neher (15). I_h was evoked by 5-s-long hyperpolarizing pulses starting from a holding potential of −50 mV and carried out in increments of −10 mV (maximal step = −120 mV). At the end of the hyperpolarizing pulse, the membrane potential was stepped to −65 mV to record tail currents. To measure the effect of neuronal activation on I_h, a base line was first obtained by recording I_h 7–10 min after reaching the whole-cell configuration; glutamate (10 μM) was then applied to the bath solution for 10–15 s, followed by recordings of I_h (voltage steps were applied from resting holding potential to −100 mV) in intervals of 5 min. Recordings were made at 30–32 °C.

The amplitude and kinetic properties of I_h were analyzed using Clampfit 9.2, Origin 6 (OriginLab), and GraphPad PRISM 2.0 (GraphPad). Final graphs were produced in Igor Pro (Wavemetrics). Current amplitude was determined by subtracting the instantaneous current at the beginning of the voltage step from the sustained component at the end of the pulse. To determine the time constants of I_h activation, a double exponential function was used, applying the Chebyshev fitting routine of Clampfit 9.2. For analysis of activation curves, the tail current amplitudes were normalized to the maximal tail current amplitude evoked by a command potential of −120 mV and plotted against the corresponding precedent command potential. The resulting data points were fit with a Boltzmann equation. Statistical significance was assessed using Student's *t* test (two-tailed, unpaired), the Mann-Whitney test, or analysis of variance, as indicated. Data are presented as means ± S.E.

Hippocampal Organotypic Slice Cultures and Biotinylation Assay

Organotypic hippocampal slice cultures were prepared from P8 Sprague-Dawley rats, using previously described methods (8, 16). On DIV 6–7, sister cultures were exposed to phosphate-buffered saline (controls) or to 50 μM L-glutamate for 10 min at 36 °C. Slice cultures were then washed quickly with ice-cold phosphate-buffered saline (pH 7.4), followed by a 30-min incubation with 2 mM Sulfo-NHS-SS-biotin (Pierce) at 4 °C. Excess biotin was quenched with 100 mM glycine in Tris-buffered saline, and the tissue was homogenized in lysis buffer composed of 50 mM Tris-HCl, pH 8.0, 150 mM NaCl, 5 mM EDTA, 1% Triton X-100, and protease inhibitor mixture. One-third of the protein sample was reserved (−80 °C; representing the total pool of both surface and intracellular protein), and the remaining two-thirds were precipitated with ImmunoPure immobilized Streptavidin beads (Pierce) at 4 °C. Western blots were performed as previously described (16, 17), using the following primary antibodies: monoclonal mouse anti-HCN1 (1:500; NeuroMab), rabbit anti-HCN2 (1:2000; Alomone), rabbit anti-Kv4.2 (1:2000; Abcam), anti-actin (1:200,000), and anti-synaptophysin (1:200,000). Signal intensities were analyzed using ImageTool software (University of Texas Health Science Center). The quantified data ($n = 6$, 4, and 3 independent experiments for HCN1, HCN2 and Kv4.2, respectively) were pooled and averaged and are presented as the normalized ratio of surface/total channels, with mean ± S.E.

RESULTS

Characterization of HCN1-GFP Expression and Function in Cultured Hippocampal Neurons—To study the trafficking dynamics of HCN1 channels in neurons directly, we established a system that enables pharmacological manipulations and good optical access while preserving the basic properties of a neuronal system (imposed by the unique polarized morphology of neurons and their patterns of electrical activity). We utilized primary hippocampal neuronal culture, where many of the *in vivo* properties of neurons are recapitulated, and which has been instructive in numerous studies of trafficking and membrane expression of both native and transfected neuronal ion channels (18, 19). In the developing rat hippocampus, HCN1

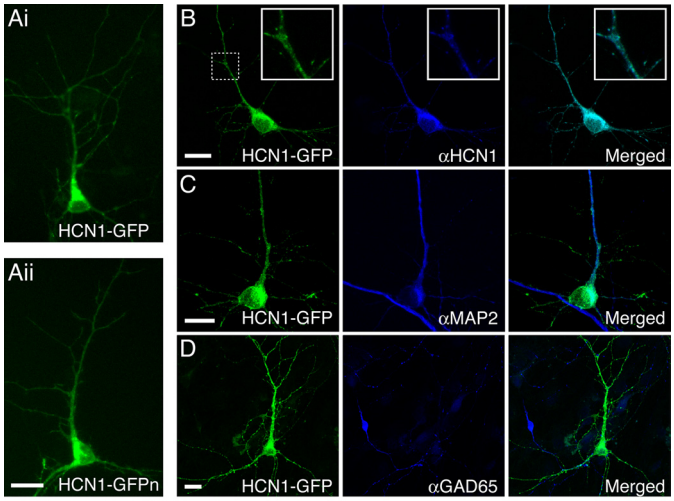

FIGURE 1. **Expression pattern of HCN1-GFP channel protein in hippocampal neurons.** *A*, images of live neurons transfected with GFP-fused HCN1 constructs. Patterns of C terminus (*top*) and N terminus (*bottom*) GFP-fused HCN1 channel expression were similar. *B–D*, confocal images of HCN1-GFP-transfected neurons. *B*, a monoclonal HCN1 antibody (αHCN1)-generated signal that co-localized with the GFP signal emitted directly from the HCN1-GFP molecules. Similar results were generated using a commercial anti-HCN1 serum (supplemental Fig. 2). *Insets*, higher magnification of a segment of a dendrite. *C*, labeling with an antibody against MAP-2, a dendritic marker, revealed that HCN1-GFP channel protein was expressed along dendrites. *D*, HCN1-GFP was expressed in principal neurons, as indicated by the lack of its co-localization with a GAD-65 antibody. Note the GAD-65-positive bipolar shaped neuron adjacent to the HCN1-GFP transfected, GAD-65-negative cell. *Scale bars*, 10 μm. The similarity between the expression pattern of HCN1-GFP and native HCN1 channels is apparent when comparing this figure to supplemental Fig. 1.

protein expression can be detected as early as P1–2 (20, 21), and substantial levels of channel protein are found in dendrites of principal neurons starting from the 2nd week of life (8, 20, 21). In line with these *in vivo* observations, immunoreactive HCN1 channels were detected in both somata and dendrites of cultured hippocampal neurons during the 2nd, 3rd, and 4th week in culture (supplemental Fig. 1).

To visualize HCN1 channels in *live* neurons, we transfected DNA plasmids that encode GFP-fused HCN1 channel proteins. To control for possible interferences of the GFP moiety with channel function or trafficking, we used two independent channel constructs in which a GFP molecule was attached to either the C or N terminus of the channel (termed HCN1-GFP and HCN1-GFPn, respectively). Both constructs had similar expression patterns in transfected neurons, as evident by the direct emission of GFP signal (Fig. 1*A*), which was distributed in both somata and processes. Immunolabeling of transfected neurons with two separate HCN1 antisera (see "Experimental Procedures") resulted in an overlap of the GFP signal with HCN1 immunoreactivity (Fig. 1*B* and supplemental Fig. 2), confirming that the GFP signal in these neurons was derived from the presence of HCN1-GFP channel proteins. Immunostaining of HCN1-GFP-transfected neurons with the dendritic marker MAP2 demonstrated that HCN1-GFP localized to dendrites (Fig. 1*C*). Because we aimed to study the HCN1 trafficking in pyramidal cells, we confirmed that HCN1-GFP molecules were expressed in this type of neurons. Immunostaining against the interneuronal marker GAD-65 revealed that the majority of the neurons in culture (22) as well as the neurons that expressed HCN1-GFP were GAD-65-negative and possessed a typical pyramidal-like shape (Fig. 1*D*; see supplemental Fig. 2 for the less frequent expression of HCN1-GFP in interneurons).

To test if the transfected HCN1-GFP molecules in principal hippocampal neurons were expressed on the cell membrane and formed functional channels with properties of endogenous HCN1, we conducted whole-cell recordings of transfected and non-transfected neurons and compared their responses to hyperpolarizing voltage steps. Measuring whole-cell responses of non-transfected neurons to hyperpolarizing steps resulted in I_h with properties similar to those observed in hippocampal neurons *in vivo* at matching developmental stages (21, 23) and which most likely represent the contribution of both HCN1 and HCN2 channels (Fig. 2) (20, 21, 23). Neurons expressing HCN1-GFP possessed a large I_h (maximal amplitude = −535 ± 107 pA; current density = −14.12 pA/picofarad; n = 12; Fig. 2, *B* and *C*, and Table 1), that was significantly augmented compared with the I_h recorded in non-transfected neurons ($F = 6.964$, $p < 0.01$, one-way analysis of variance). Further analysis of I_h in transfected neurons revealed biophysical properties similar to those previously reported for channels composed of cloned HCN1 subunits (4, 24); activation kinetics were best fit to a double-exponential function and showed the typical acceleration at more hyperpolarized membrane potentials (Fig. 2*D* and Table 1). The gating properties of I_h in neurons expressing HCN1-GFP were assessed by plotting a tail current activation curve fit by the Boltzmann equation (see "Experimental Procedures"). This yielded a $V_{½}$ value of −77.1 ± 2.6 mV (Fig. 2*D* and Table 1), in general accord with previous reports on the gating properties of channels composed of HCN1 subunits in heterologous systems co-transfected with the neuronal HCN1-interacting protein TRIP8b; $V_{½}$ values of −75 to −78 mV were reported by one study (12), and values ranging from −71 to −75 mV were reported by another (25). In addition, both native I_h and the current generated in HCN1-transfected neurons were inhibited by extracellular Cs^+ (1–2 mM; Fig. 2*A* and supplemental Fig. 3), as established for this conductance (4). The membrane input resistance of HCN1-GFP-expressing neurons was reduced (Table 1), as expected for neurons in which I_h was up-regulated (4, 10, 11). Both the expression pattern and the functional properties of the HCN1-GFPn construct were similar in N and C terminus-fused HCN1-GFP, demonstrating that the site of GFP insertion did not influence channel expression and function (supplemental Fig. 4). Thus, in cultured hippocampal neurons, GFP-fused HCN1 channels were delivered to the cell membrane and possessed functional properties typical of cloned, untagged HCN1 channels.

Analysis of HCN1-GFP Channel Trafficking in Live Neurons—HCN1-GFP channel proteins expressed in neurons were distributed along dendrites in a mixed punctate-diffuse pattern that recapitulated the expression pattern of endogenous HCN1 channels (Fig. 3, *A* and *B*). Visualizing GFP-fused HCN1 channel protein in live neurons using time lapse imaging techniques, we found that many of the HCN1-containing puncta traveled along dendrites (Fig. 3, *C* and *D*, and supplemental Movies S1 and S2) as well as in the perisomatic region (supplemental Movie S3). Analysis of over 1500 puncta from 11 neurons revealed that 27.7 ± 5.1% of the puncta were mobile (mean velocity = 0.13 ± 0.01 μm/s; Fig. 3*E*). Mobile puncta exhibited several patterns of movement; the majority traveled bidirec-

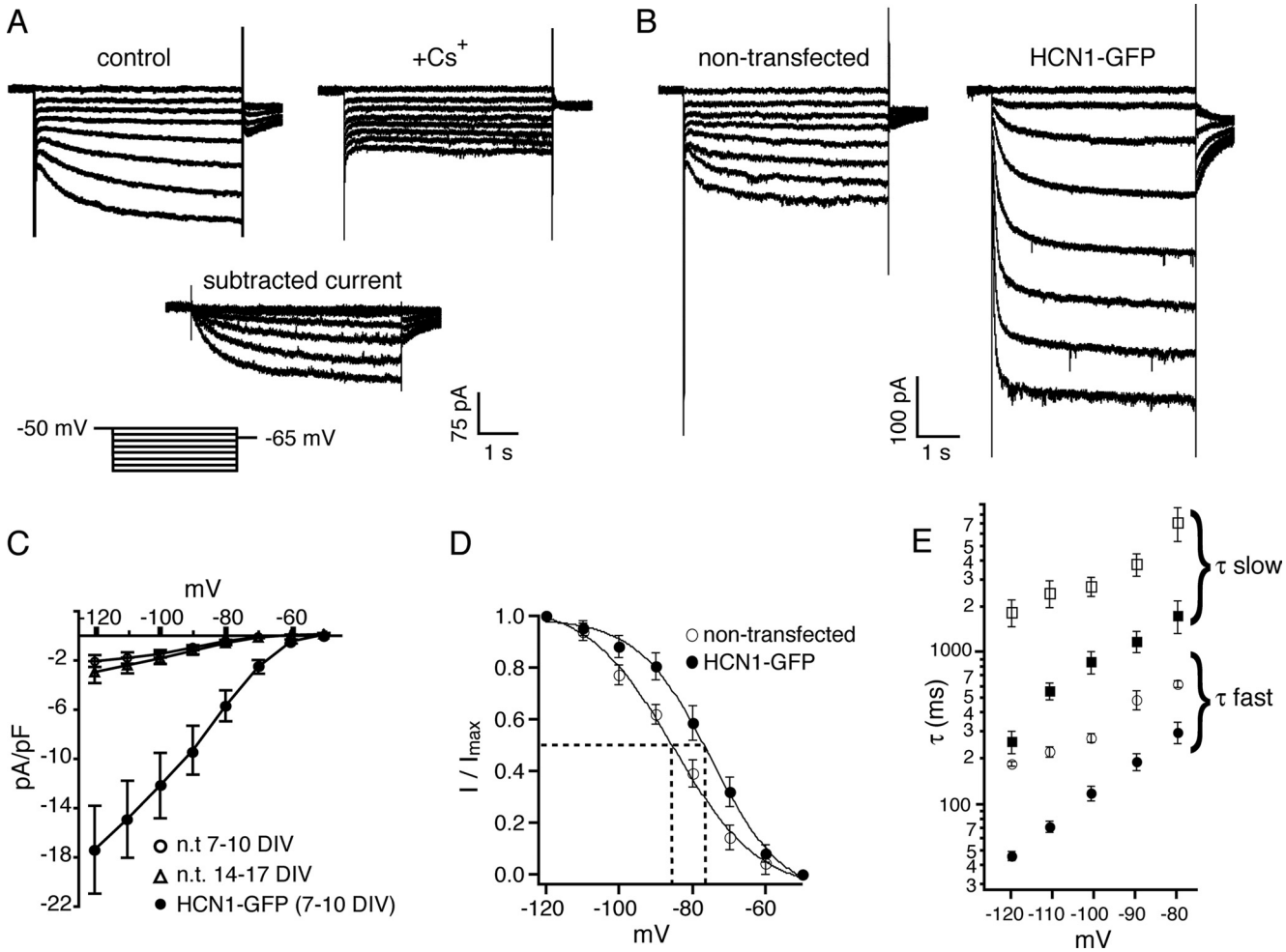

FIGURE 2. **Properties of native I_h in non-transfected hippocampal neurons, compared with current properties in HCN1-GFP-transfected neurons.** *A*, examples of whole-cell traces of hyperpolarization-activated currents from naive, non-transfected neurons (3rd week *in vitro*). Application of hyperpolarizing voltage steps resulted in a typical slowly developing inward current that was sensitive to Cs^+ (1 mM). *B*, transfection of HCN1-GFP resulted in augmented I_h, compared with non-transfected, same age neurons (DIV 9–10). *Traces* represent whole-cell, unsubtracted currents. *C*, I_h current density in HCN1-GFP-transfected neurons (DIV 7–10; $n = 12$) was significantly higher than in non-transfected (*n.t.*) neurons of the same age ($n = 8$ I_h-positive cells; note that at this age only 36% of cells had detectable I_h), and DIV 14–17 ($n = 11$). *D*, activation curves from cells transfected with HCN1-GFP showed a depolarizing shift, consistent with I_h composed primarily of HCN1 channels. *E*, I_h kinetics in transfected (*filled symbols*) and non-transfected (*empty symbols*) neurons. The faster kinetics in transfected neurons is consistent with a primarily HCN1-mediated I_h. Values are mean ± S.E. See "Experimental Procedures" for details of the analyses.

TABLE 1

Comparison of I_h properties in neurons transfected with the HCN1-GFP construct and non-transfected neurons of two age groups

Both kinetic and gating properties of I_h in non-transfected neurons were consistent with a mixed I_h contributed to by HCN1 and HCN2 subunits. Neurons transfected with HCN1-GFP exhibited faster kinetics and more depolarized gating properties, consistent with a current mediated primarily by the HCN1 channel subunit.

	Non-transfected (2nd week in culture)	Non-transfected (3rd week in culture)	HCN1-GFP (2nd week in culture)
$V_{½}$ (mV)	−83.7 ± 2.4 ($n = 5$)	−85.2 ± 2.3 ($n = 10$)	−77.1 ± 2.6[a] ($n = 12$)
Slope factor	11.7 ± 0.7 ($n = 5$)	11.6 ± 0.1 ($n = 10$)	10.9 ± 0.2 ($n = 12$)
τ fast (ms) at −120 mV	197 ± 55 ($n = 5$)	185 ± 6 ($n = 5$)	46 ± 3[a] ($n = 12$)
τ slow (ms) at −120 mV	1314 ± 588 ($n = 5$)	1831 ± 369 ($n = 5$)	260 ± 42[a] ($n = 12$)
Rm (megaohms)	437 ± 8.2 ($n = 9$)	330 ± 38 ($n = 12$)	290 ± 28[a] ($n = 14$)
I_h density (pA/picofarad), at −120 mV	−1.97 ± 0.58 ($n = 8$)	−2.39 ± 0.48 ($n = 11$)	−14.12 ± 2.16[a] ($n = 12$)

[a] Significantly different ($p < 0.05$) in comparison with non-transfected neurons at the 2nd week in culture.

tionally, whereas others moved in one direction only (Fig. 3, *D* and *F*). Different patterns were also found in the continuity of motion; a small subpopulation traveled continuously, whereas most were immobile for relatively long periods, interspersed with bursts of movement. Interestingly, the frequency and duration of puncta mobility correlated with directionality; the same subpopulation of puncta that tended to move continuously traveled unidirectionally over relatively long dendritic distances, whereas puncta with little or fragmented motion typically traveled bidirectionally (Fig. 3*G*). The mobility of HCN1-GFP-containing puncta was independent of the site of GFP insertion (see supplemental Fig. 4). Trafficking dynamics of the HCN1-GFP channels differed significantly from that of channels composed of HCN2 subunits, a distinct channel isoform that is also expressed in hippocampal neurons; HCN2-GFP distribution was less punctate, a smaller proportion of the HCN2-

GFP puncta were mobile, and mobile puncta traveled shorter distances and had longer pause periods (Fig. 4). These distinctive properties of each of the HCN channel isoforms persisted when both isoforms were co-transfected in a single neuron (Fig. 4, *F* and *G*).

To examine if the mechanisms of the trafficking of HCN1 channels in neurons involved actin and/or microtubules, we analyzed the mobility of HCN1-GFP-containing puncta in transfected neurons following pharmacological manipulation of these cytoskeletal networks. Incubation with the microtubule depolymerizing agent nocodazole (10 μM, 30 min) selectively disrupted the integrity of the tubulin network, as evident by the substantial reduction in α-tubulin immunoreactivity, but did not disrupt phalloidin labeling of F-actin (Fig. 5*A*). Although the number and distribution of total HCN1-GFP puncta in transfected neurons were not influenced by nocodazole treatment (Fig. 5*B*), the fraction of *mobile* puncta was reduced ($p < 0.05$; Fig. 5*C*). Interestingly, nocodazole-treated cells exhibited a specific reduction in the fraction of puncta that moved relatively long distances (defined as a displacement of at least 8 μm during a 2-min imaging session; Fig. 5*D*). Thus, the population of puncta that remained mobile after nocodazole treatment (~50% of the original mobile population; Fig. 5*C*) exhibited a reduction in the total distance traveled from 7.08 ± 0.73 μm before treatment to 4.65 ± 0.55 μm ($n = 137$ mobile puncta; $p < 0.05$).

Upon application of the cell-permeable toxin jasplakinolide (0.5 μM, 30 min), a selective stabilizer of actin filaments (26, 27), phalloidin labeling of F-actin in neurons was markedly reduced, as expected because of the competition between jasplakinolide and phalloidin for the same actin binding site (26, 27). Jasplakinolide did not influence α-tubulin immunoreactivity (Fig. 5*A*), suggesting that in these experiments, jasplakinolide was efficiently bound to F-actin without interrupting the microtubule network. Disruption of F-actin dynamics reduced the fraction of mobile HCN1-GFP puncta by ~75% ($p < 0.05$; Fig. 5*C*). However, unlike nocodazole, jasplakinolide reduced the population of mobile puncta without altering the average distance traveled by the remaining mobile population (5.53 ± 0.51 μm before treatment *versus* 5.61 ± 0.85 after treatment; $n = 158$ mobile puncta; $p > 0.05$; Fig. 5*D*). Treatment with the DMSO (0.06%)

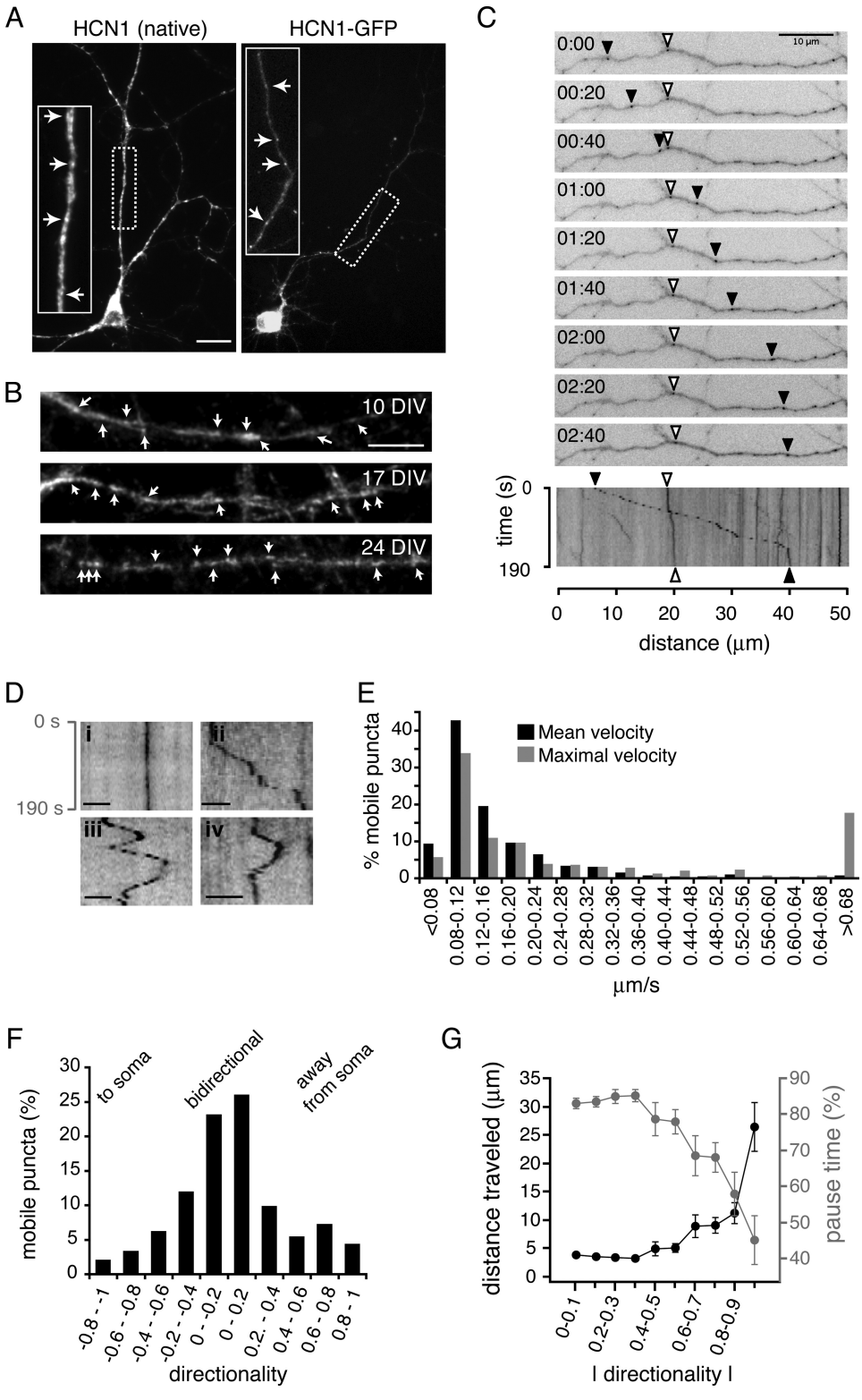

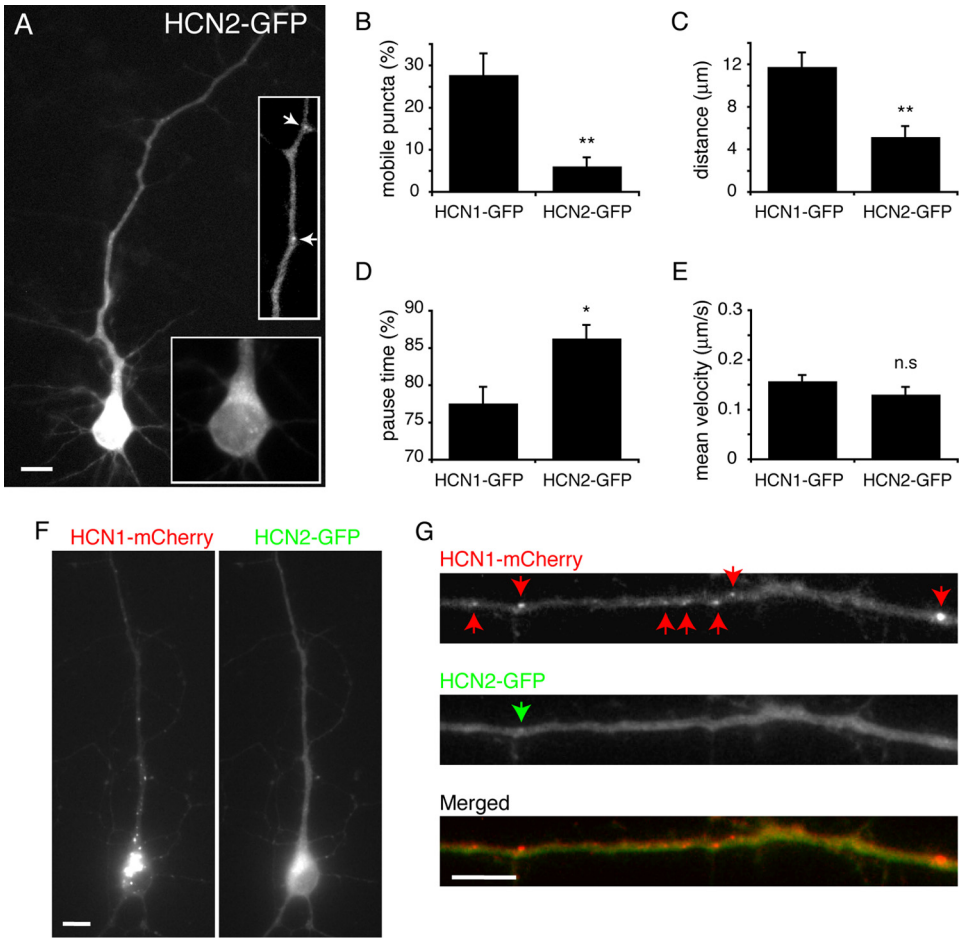

FIGURE 4. **Isoform specificity of the expression and trafficking patterns of the HCN1 and HCN2 channel isoforms.** *A*, an image of the GFP signal emitted by a live neuron (9 DIV), 26 h after transfection with the HCN2-GFP channel construct. Whereas, similar to HCN1-GFP, HCN2-GFP expression was apparent in soma and dendrites, the distribution pattern of HCN2-GFP was more diffuse, with fewer identifiable puncta (for a comparison, see live neuron expressing HCN1-GFP in Fig. 3*A*). *B*, analysis of 498 dendritic HCN2-GFP puncta from six cells (derived from three independent experiments with separate cultures) revealed that only a small subpopulation of HCN2-GFP puncta was mobile (6.1% ± 2.1%), significantly less than for HCN1-GFP (27.7% ± 6.1%). *C–E*, the small subpopulation of mobile HCN2-GFP puncta traveled smaller distances compared with HCN1-GFP, as quantified by the mean total distance traveled during the 190-s imaging period (*C*). The reduced mobility of HCN2-GFP puncta coincided with their longer stationary periods (*D*), whereas mean velocity corrected for immobile periods did not differ between HCN1- and HCN2-GFP puncta (*E*). *F*, the isoform-specific distribution of HCN1- and HCN2-GFP channels persisted when they were co-transfected in the same neurons; in a live neuron co-transfected with mCherry-fused HCN1 and GFP-fused HCN2 at a 1:1 cDNA ratio, HCN1 molecules were distributed in a more punctate pattern when compared with HCN2. *G*, an *enlarged image* of a dendritic segment taken from the cell in *F*. Puncta are indicated by *arrows*. Values are expressed as mean ± S.E. *, $p < 0.05$; **, $p < 0.01$, unpaired two-tailed *t* test; *n.s.*, non-significant effect. *Scale bars*, 10 μm.

vehicle did not affect the fraction of mobile puncta (Fig. 5*C*) or their mobility patterns. These results indicate that intact microtubule and actin networks are essential for the trafficking of populations of HCN1 channels in neurons.

Regulation of HCN1-GFP Trafficking by Ionotropic Glutamate Receptor Activation—We next studied if neuronal stimulation regulated HCN1 channel trafficking. Application of the excitatory amino acid L-glutamate (10 μM) resulted in a rapid inhibition of HCN1-GFP motion (Fig. 6 and supplemental Movie S4) in 17 of 18 neurons. This reduction of the proportion of moving puncta commenced within 1 min following glutamate application and persisted in the presence of glutamate (Fig. 6*B*). Glutamate-induced arrest of mobility was reversible; by 30 min following the removal of glutamate from the bath solution, the mobility of HCN1-GFP-containing puncta returned to base levels (Fig. 6*D* and supplemental Movie S5). Vehicle treatment did not influence puncta mobility (Fig. 6, *B* and *E*), indicating that potential artifacts from the application procedure or from reduced neuronal viability (*e.g.* from phototoxicity) were unlikely to account for the observed effect of glutamate on HCN1-GFP-puncta movement. The inhibitory effect of glutamate on HCN1 mobility required activation of ionotropic receptors; application of 10 μM glutamate in the presence of the specific NMDA receptor blocker amino-5-phosphonovaleric acid (100 μM) or

FIGURE 3. **Dynamics of HCN1 channel trafficking in dendrites.** *A*, a mature (25 DIV), non-transfected hippocampal neuron immunolabeled with HCN1 antibody (*left*), exhibiting a typical mixed punctate-diffuse pattern of dendritic HCN1 expression. The distribution of HCN1-GFP in transfected neurons recapitulated this pattern, as demonstrated by a transfected neuron imaged live (*right*). *B*, the dendritic distribution of native HCN1 in primary hippocampal neurons was apparent at different ages (10–24 DIV), as shown by immunolabeling of non-transfected neurons with a specific HCN1 antibody (9). *C*, *upper panels*, time-lapse images of HCN1-GFP puncta along a dendritic segment. Fast moving (*filled arrowhead*) and slow moving (*empty arrowhead*) puncta are indicated. *Lower panel*, Kymograph summarizing puncta movement during 190 s in the dendritic segment shown in the *upper panel*. *D*, *kymograph* of a static punctum (*i*) and of three examples of mobile puncta that exhibited either unidirectional (*ii*) or bidirectional trajectories (*iii* and *iv*). Movement of puncta was often interspersed with periods of immobility (*ii* and *iv*). *Scale bar*, 4 μm. *E*, mean velocity (corrected for immobile periods) and maximal velocity (defined as the fastest movement recorded per punctum) in the population of HCN1-GFP-containing puncta. *F*, directionality distribution of mobile puncta. The directionality index represents the relative amount of time in motion in a direction toward or away from the soma over the total mobile time (see "Experimental Procedures"). *G*, correlation between directionality and continuity of the movement of HCN1-GFP puncta. *Black symbols* refer to the *left y axis*, which represents the mean distance traveled by a given punctum during the imaging session (190 s), and *gray symbols* refer to the *right y axis*, which represents the mean percentage of time in which the puncta were immobile. Puncta that moved bidirectionally (and therefore had low values of "absolute directionality"; see "Experimental Procedures") tended to cover shorter distances and to experience longer periods of immobility compared with puncta that moved unidirectionally (high values of absolute directionality). Analyses in *E–G* were based on 384 mobile puncta from 11 neurons derived from five independent cultures. Values are mean ± S.E. *Scale bars* in *A* and *B*, 10 μm.

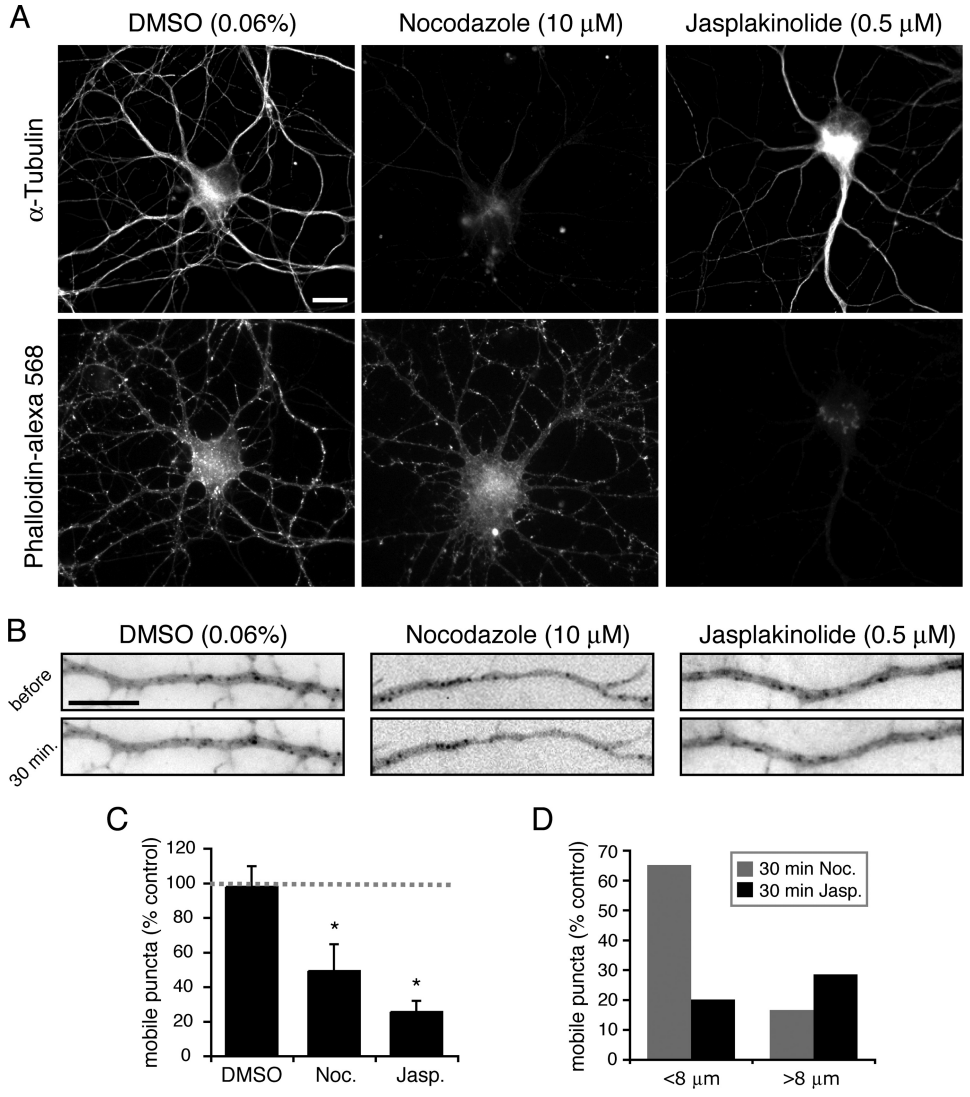

FIGURE 5. **Involvement of the actin and microtubule networks in the trafficking of HCN1 channels.** *A*, images of neurons double-stained with a monoclonal anti-α-tubulin antibody (*upper panel*) and Alexa-568-conjugated phalloidin (to label F-actin). Immunoreactivity to α-tubulin was markedly reduced following a 30-min incubation with the microtubule disrupter nocodazole, whereas actin labeling in the same cell was intact. Conversely, incubation of neurons with jasplakinolide, an actin-stabilizing drug that competes with phalloidin for the same actin binding site resulted in substantial reduction of the phalloidin signal (indicative of potent binding of the drug to its target) and did not alter α-tubulin immunoreactivity in the same cell. *B*, images of HCN1-GFP signal in dendritic segments of live transfected neurons before and after treatment show a lack of significant reduction in the number of HCN1-GFP puncta. *C*, comparison of the fraction of mobile puncta before and after treatment with DMSO (vehicle), nocodazole (*Noc.*), or jasplakinolide (*Jasp.*). For each cell, the fraction of mobile puncta was calculated before and after treatment (paired *t* test; *, $p < 0.05$) and then normalized to the pretreatment value. *D*, mobile puncta were categorized to long distance (>8 μm) and short distance moving, based on the distance they traveled during the 2-min imaging session. This dichotomization demonstrated the preferential reduction in long distance movement following nocodazole but not jasplakinolide treatment. Data are based on tracking of 486 mobile puncta from 4–5 cells/experimental group. *Scale bars* in *A* and *B*, 10 μm.

the specific AMPA receptor blocker 6-cyano-7-nitroquinoxaline-2,3-dione (50 μM) fully blocked the glutamate-induced halt of HCN1-GFP mobility (Fig. 6*E*). These experiments indicate that both NMDA and AMPA receptor activation contributed to the suspension of HCN1 channel trafficking. The involvement of calcium in this process was supported by the fact that eliminating calcium from the bath solution abolished the effect of glutamate on HCN1-GFP puncta mobility (Fig. 6*E*).

Increased Glutamatergic Input Up-regulates the Surface Expression of Transfected HCN1—To test if glutamate-receptor activation resulted in increased surface expression of transfected HCN1 channels, we used an HCN1 channel construct tagged with an extracellular HA recognition sequence (see "Experimental Procedures"). The expression pattern of HA-HCN1 channels in neurons was similar to that of the HCN1-GFP construct (Fig. 7*A*). To differentiate between surface-expressed and intracellular HA-HCN1 channels, we first incubated live neurons with a monoclonal anti-HA antibody under non-permeabilizing conditions to visualize surface channels. This was followed by fixation, membrane permeabilization, and incubation with a different anti-HA antibody, to visualize the remaining intracellular HA-HCN1 channels (see "Experimental Procedures"). Exposure of HA-HCN1-expressing neurons to 10 μM glutamate for 10 min led to marked augmentation of the surface-expressed channel signal in both somatic and dendritic compartments (Fig. 7, *B–E*). These results indicate that HA-HCN1 channel proteins resided in both intracellular and surface domains and that increased excitatory input significantly augmented their surface expression.

Increased Glutamatergic Input Augments Surface Expression of Native HCN1 in a Reversible Manner and Up-regulates I_h—Trafficking of overexpressed, exogenous proteins may not fully recapitulate transport of native proteins. In addition, adding a molecular tag, such as HA or GFP, might lead to structural changes that influence the interaction of the HCN channel with other proteins. To address these potential caveats, we examined the effects of glutamate application on both the surface expression and the function of native hippocampal HCN1 channels.

Whole-cell recordings of non-transfected neurons revealed the augmentation of I_h amplitude within minutes following glutamate application (Fig. 8, *A* and *B*), consistent with previous reports on the activity dependence of I_h in brain slice preparations (10, 11). Using biotinylation of endogenous surface proteins in cultured hippocampal slices, we found that surface expression of HCN1 channels was significantly elevated following 10 min of glutamate exposure (2.6 ± 0.7-fold increase, $n = 6$ experiments; Fig. 8, *C* and *D*). This effect was isoform-specific,

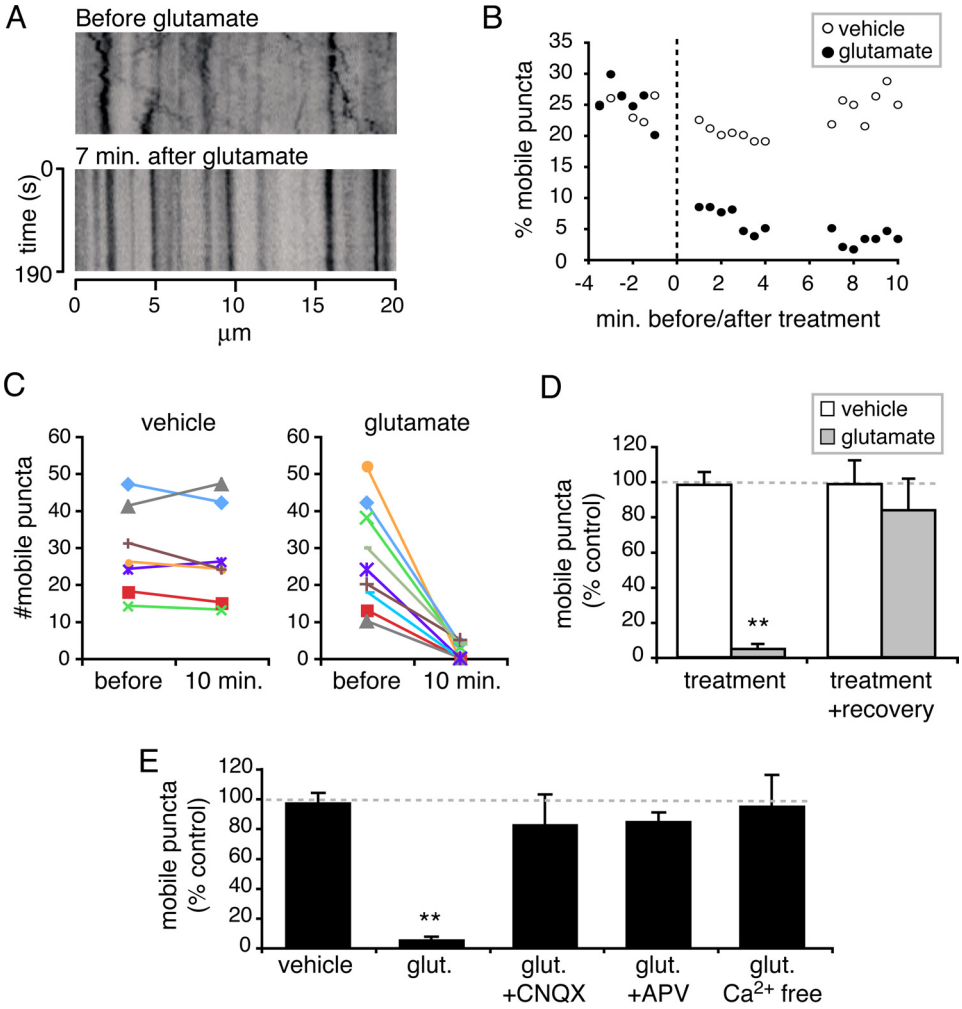

FIGURE 6. **HCN1 channel trafficking is reversibly arrested by activation of ionotropic glutamate receptors by an extracellular calcium dependent mechanism.** *A*, *kymographs* representing HCN1-GFP puncta movement in dendrites and its inhibition by 10 μM glutamate. *B*, time course of glutamate-induced arrest of HCN1 channels; quantitative analysis of puncta movements in two representative neurons (vehicle and glutamate-treated) before as well as during the 1–4 min epoch and the 7–10 min epochs after treatment. Drastic suppression of puncta mobility was apparent already at 1 min post-glutamate and persisted for at least 10 min, whereas no reduction of movement occurred in vehicle-treated neurons. *C*, quantitative analysis of the number of mobile puncta in neurons exposed to 10 μM glutamate or to vehicle treatment for 10 min. Paired data points represent the number of mobile puncta in the same neuron before and after treatment. *D*, the reduction in the fraction of mobile puncta at 10 min post-glutamate (*gray column* in the *left column pair*) was reversed after an additional recovery period of 30 min. At that time point, the fraction of mobile puncta (*gray column* in the *right pair of columns*) did not differ significantly from the pretreatment value (*blank column*). There was no significant change in puncta mobility in vehicle-treated neurons throughout the duration of the experiment. *E*, in the presence of either the AMPA receptor blocker 6-cyano-7-nitroquinoxaline-2,3-dione (*CNQX*) or the NMDA receptor blocker amino-5-phosphonovaleric acid (*APV*), glutamate (*glut.*) no longer arrested puncta mobility ($p > 0.05$). In addition, application of glutamate in a calcium-free solution failed to suppress HCN1-puncta mobility. Puncta were tracked in 4–9 neurons/group (>7000 puncta in total). *Bars*, mean ± S.E. **, $p < 0.01$ (paired *t* test).

because no significant change in membrane expression was found for the HCN2 channel isoform. In addition, surface expression of the voltage-gated potassium channel Kv4.2 did not change significantly following glutamate application, although a trend for its reduction was observed, consistent with previous studies (28). The glutamate-induced increase in surface HCN1 channels was transient, resolving within 5 h (Fig. 8, *C* and *D*).

DISCUSSION

In this study, we employed live imaging techniques to examine the trafficking of HCN channels in hippocampal neurons. We found that both transfected and endogenous HCN1 channels resided in vesicle-like dendritic structures. HCN1-GFP puncta traveled rapidly, and their trafficking was arrested within minutes by disruption of the cytoskeletal network or activation of ionotropic glutamate receptors. Glutamate-induced arrest of HCN1-GFP channels coincided with increased surface expression of both transfected and native channels and with augmented I_h.

The current experiments visualized HCN channels directly and employed live imaging to characterize their trafficking and its regulation in live neurons. HCN1 channels have been expressed and studied extensively in heterologous systems (29–33), which enabled the characterization of their biophysical properties and basic regulatory mechanisms. However, heterologous expression systems may not capture the full complexity of channel behavior and regulation in neurons. For example, activity-dependent heteromerization of HCN channel isoforms cannot be studied in non-neuronal cells because heteromerization in these cells is almost non-selective (16, 32). In addition, studying *activity*-dependent regulation of channel trafficking and surface expression depends on membrane excitability and thus requires neuronal systems. Expression of HCN channels in hippocampal neurons, as described here, enables study of the repertoire of regulatory mechanisms of these channels.

The use of HCN1-GFP channels might raise questions regarding the similarities between native and transfected channel behavior. As described above, the distribution and properties of HCN1-GFP in primary hippocampal neurons recapitulated most but not all of the features of native HCN1 channels *in vivo*. Thus, exogenous HCN channels generated I_h, indicating that they were inserted within the membrane in a functional manner. Notably, the properties of I_h in neurons that overexpressed HCN1-GFP were consistent with those of channels composed of the HCN1 subunit, which is the major subunit in adult hippocampal CA1 pyramidal cells. Whereas heteromerization of HCN1/HCN2 isoforms may differ in native cells and those transfected with HCN1, the regulation of HCN1 channel trafficking by the auxiliary protein TRIP8b in dissociated hippocampal cultures was similar to that found *in vivo* (12, 32). The dendritic distribution

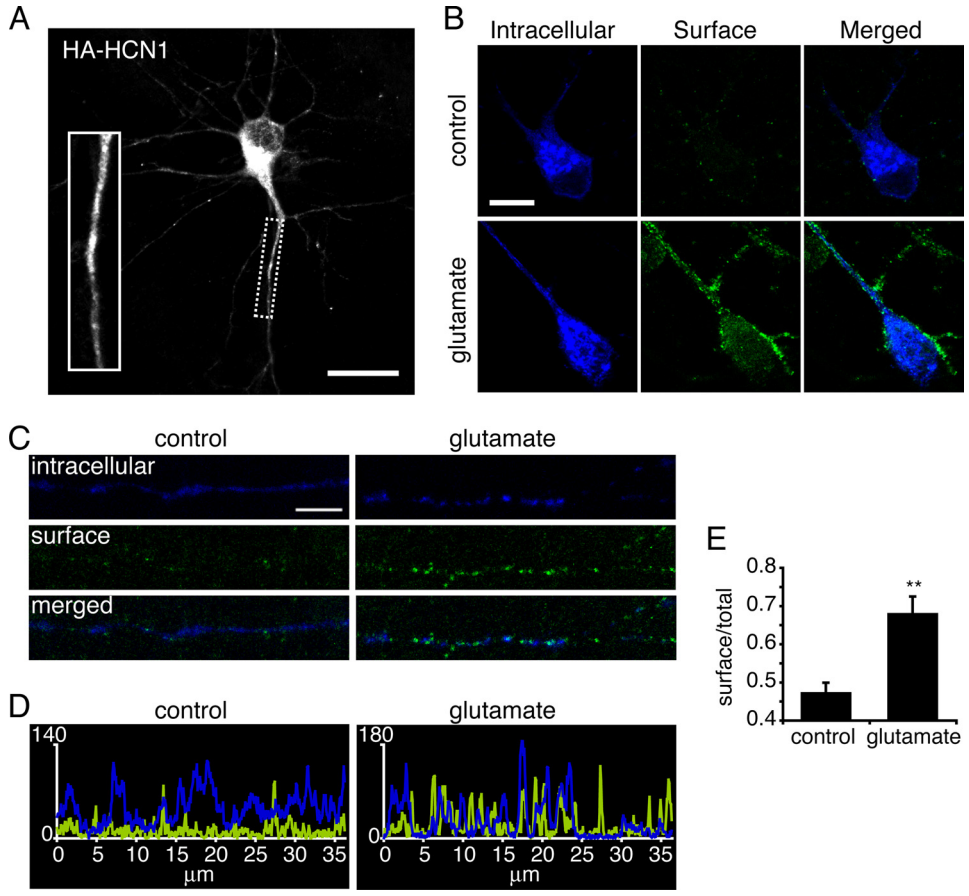

FIGURE 7. **Glutamate-dependent surface expression of HCN1 channels.** *A*, distribution pattern of total (intracellular + surface) HA-tagged HCN1 protein expressed in a hippocampal neuron as visualized using a monoclonal anti-HA antibody under cell-permeable conditions. Similar to the HCN1-GFP construct, HA-HCN1 was distributed in a mixed diffuse-punctate pattern. *B* and *C*, selective immunolabeling of surface HA-HCN1 (see "Experimental Procedures") revealed a punctate surface pattern in both dendrites and somata; application of 10 μM glutamate increased the ratio of surface to intracellular puncta in both perisomatic regions (*B*) and dendrites (*C*). *D*, the increase in surface HA-HCN1 puncta in dendrites was demonstrated using a line plot (*y axis* shows arbitrary intensity units, 0–255), representing the dendritic segments shown in *C*. In *B–D*, a vehicle-treated control neuron was compared with a glutamate-treated cell, and the ratios of surface (*green*) HCN1-HA channels/total channel signal for the cell (*green* + *blue*) were compared. *E*, quantitative summary of HA-HCN1 surface expression. Analysis was based on three independent experiments, each performed at a minimum in duplicate (see "Experimental Procedures"). Values are mean ± S.E. **, $p < 0.01$ (unpaired *t* test). *Images* in *B* are confocal images with a virtual slice thickness (*z*) of <1 μm; *images* in *C* are stacked representations of two virtual sections. *Scale bars*, 20 μm (*A*) and 5 μm (*B* and *C*).

of both transfected and endogenous HCN1 channels in dissociated hippocampal neurons did not show the distal/proximal gradient found in CA1 hippocampal pyramidal cells *in vivo* (6, 34, 35). This is not surprising; the establishment and maintenance of the somatodendritic gradient requires long term excitatory input from the temporoammonic pathway (9), and this laminated input is absent in primary hippocampal cultures.

Neuronal expression of GFP-fused HCN1 channels was compared with that of the HCN2 isoform. In the rodent hippocampus, both HCN1 and HCN2 channel subunits are expressed, often in the same neurons (35, 36), and can form either homomeric or heteromeric channel complexes (32, 36) with distinct functional properties (37, 38). *In vivo*, there are several lines of evidence for differential regulation of the HCN1 and HCN2 isoform trafficking. For example, different spatiotemporal distribution patterns of these subunits have been found in the developing hippocampus, and their expression is differentially regulated by seizure activity (20, 35). Recent studies have reported differences in the regulation of HCN1 and HCN2 by the auxiliary protein TRIP8b, which influences surface expression of these channels (25, 39). Accordingly, we found here isoform-specific trafficking dynamics; HCN2-containing puncta had overall reduced mobility compared with HCN1-containing puncta. In addition, unlike HCN1, surface expression of the native HCN2 isoform was unaltered after exposure to glutamatergic excitation. These findings raise the possibility that the distinctive regulation of HCN1 and HCN2 channel trafficking and surface expression are a result of differential interaction with auxiliary proteins (33).

Activation of ionotropic glutamate receptors resulted in a dramatic and rapid suspension of motion that was associated with increased surface expression, measured using selective immunolabeling of surface channels. Selective blockade of either AMPA- or NMDA-type glutamate receptors as well as removal of calcium from the bath solution abolished the inhibitory effect of glutamate on HCN1 trafficking. The contribution of both of these receptors might be sequential; glutamatergic signaling first activates AMPA receptors, leading to membrane depolarization that promotes the removal of the Mg^{2+} block from NMDA receptors. The latter facilitates ionic influx through the NMDA receptors, thus contributing to the rise in intracellular calcium levels. Alternatively, Ca^{2+}-permeable AMPA receptors have been shown to reside in dendrites of hippocampal pyramidal neurons (40, 41) and therefore may provide a direct route for Ca^{2+} influx, which may be further enhanced by NMDA receptors and other sources of calcium.

The glutamate-induced arrest of the dendritic mobility of HCN1-GFP channels was associated with an increase in their surface expression. An association between reduced or arrested protein mobility and the insertion of the same protein into the membrane has been reported in a number of studies, suggesting that vesicular insertion of intracellular protein-carrying organelles into the plasma membrane may result in the inhibition of their movement. This might be a result of the more viscous properties of the membrane compared with the cytoplasm, of the action of anchoring complexes, or both. Such an activity-dependent relationship has been established for Semaphorin 3A (42, 43) and for the ion channel TRPC5, which was

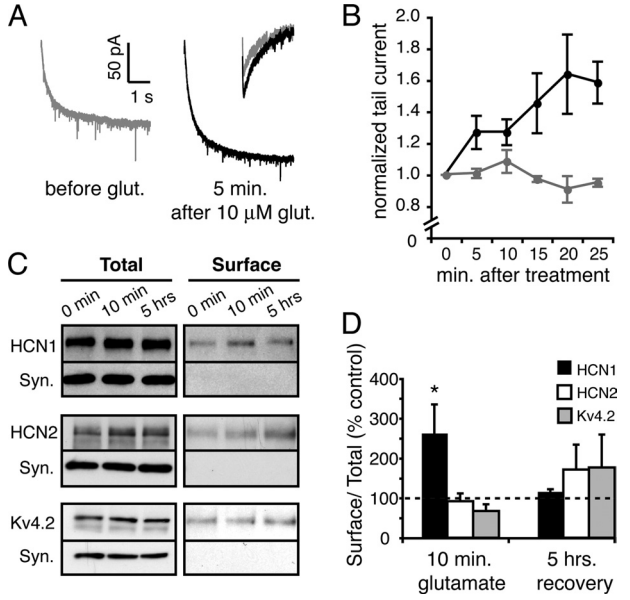

FIGURE 8. **Excitation enhances surface expression of native, functional HCN1 channels.** *A*, increased I_h amplitude shown as whole-cell responses and tail currents (*inset*) in cultured hippocampal neurons 5 min after application of the excitatory neurotransmitter glutamate, compared with preapplication. Voltage steps were applied from a holding potential of −50 to −100 mV. For presentation, the ohmic and capacitive currents at the beginning and at the end of the trace were excluded. *B*, time course of glutamate-induced augmentation of I_h (tail currents; $n = 3–6$/time point/group). *C*, biotinylation of surface-expressed, native HCN channels (see "Experimental Procedures") demonstrated that exposure to glutamate reversibly augmented surface HCN1 as a fraction of total HCN1 channels. The *three left lanes* represent total cellular HCN1 protein (intracellular + surface), whereas the *right three lanes* represent biotinylated, surface-expressed channels (as supported by the absence of the intracellular protein synaptophysin). Unlike the glutamate-dependent, reversible increase of surface HCN1 channel expression, no significant change was found in HCN2 or Kv4.2 surface expression, suggesting that excitation-induced increase of surface expression was selective. Lanes containing surface channels were loaded with 3 times the protein loaded for total protein analysis. *D*, quantification of surface/total protein ratios for HCN1, HCN2, and Kv4.2 10 min following glutamate application and after a 5-h recovery period. Values shown are mean ± S.E. (*, $p < 0.05$; two-tailed paired *t* tests).

studied in HEK293 cells (44). Future studies will attempt to examine if the same HCN1-GFP channel puncta that are arrested by glutamate are inserted into the membrane.

Although overexpression of ion channels might overwhelm or alter cellular processes, we found here that surface expression of both transfected and native, endogenous HCN1 channels was enhanced by glutamate application. Augmentation of I_h within minutes of neuronal stimulation by direct glutamate application, by θ-burst-induced LTP, or by pharmacologically induced synaptic activity has been previously reported (10, 11). This up-regulation is thought to serve an important homeostatic role; by reducing input resistance, increased I_h functions to dampen neuronal excitability in response to enhanced depolarizing input. The results of the current studies suggest that up-regulation of I_h may be accomplished via altered trafficking and increased surface expression of HCN1 channels.

The findings described above demonstrate for the first time rapid HCN1 trafficking in neurons as a dynamic process that is regulated by neuronal activity within a time scale of minutes. These channels can thus be added to the roster of ion channels whose trafficking is regulated rapidly by activity, an effect that may influence intrinsic neuronal excitability (28, 45–47). Whereas for HCN1 we found activity-dependent arrest of mobility and augmented membrane expression, the trafficking of other channels was influenced by network activity in distinct ways, including alterations of internalization (28, 46), recycling (47), or clustering (45). Thus, regulation of ion channel trafficking provides a mechanism for rapid alterations in neuronal excitability, which in turn contributes to neuronal plasticity. In addition, orchestrated co-regulation of the trafficking of several ion channels, such as HCN and potassium channels, might be the basis of the observed coordinated regulation of I_h and I_A (48, 49) or $I_{k\text{-}leak}$ (50, 51). This coordinated regulation of channels with opposing properties helps preserve neuronal properties and permit their fine tuning. Future studies will examine whether the mechanisms involved in activity-dependent trafficking and surface expression of HCN and co-regulated channels share common molecular mediators.

In summary, we demonstrate and characterize here the dynamics and activity-dependent regulation of HCN channel trafficking and surface expression in neurons. We suggest that the rapid regulation of HCN1 channel surface expression found here might provide a novel mechanism for activity-dependent changes in I_h. These, in turn, influence neuronal excitability in changing physiological and perhaps pathological contexts.

Acknowledgments—We thank Dr. B. Santoro for the N terminus-fused GFP-HCN constructs, Drs. L. Hilgenberg and J. A. van Hooft for constructive advice, and Sharib Gaffar, Indra Tjong, and Maryjane Vennat for assistance with trafficking analysis.

REFERENCES

1. Zhang, W., and Linden, D. J. (2003) *Nat. Rev. Neurosci.* **4,** 885–900
2. Beck, H., and Yaari, Y. (2008) *Nat. Rev. Neurosci.* **9,** 357–369
3. Kennedy, M. J., and Ehlers, M. D. (2006) *Annu. Rev. Neurosci.* **29,** 325–362
4. Robinson, R. B., and Siegelbaum, S. A. (2003) *Annu. Rev. Physiol.* **65,** 453–480
5. Santoro, B., and Baram, T. Z. (2003) *Trends Neurosci.* **26,** 550–554
6. Lörincz, A., Notomi, T., Tamás, G., Shigemoto, R., and Nusser, Z. (2002) *Nat. Neurosci.* **5,** 1185–1193
7. Magee, J. C. (1999) *Nat. Neurosci.* **2,** 508–514
8. Bender, R. A., Kirschstein, T., Kretz, O., Brewster, A. L., Richichi, C., Rüschenschmidt, C., Shigemoto, R., Beck, H., Frotscher, M., and Baram, T. Z. (2007) *J. Neurosci.* **27,** 4697–4706
9. Shin, M., and Chetkovich, D. M. (2007) *J. Biol. Chem.* **282,** 33168–33180
10. van Welie, I., van Hooft, J. A., and Wadman, W. J. (2004) *Proc. Natl. Acad. Sci. U.S.A.* **101,** 5123–5128
11. Fan, Y., Fricker, D., Brager, D. H., Chen, X., Lu, H. C., Chitwood, R. A., and Johnston, D. (2005) *Nat. Neurosci.* **8,** 1542–1551
12. Lewis, A. S., Schwartz, E., Chan, C. S., Noam, Y., Shin, M., Wadman, W. J., Surmeier, D. J., Baram, T. Z., Macdonald, R. L., and Chetkovich, D. M. (2009) *J. Neurosci.* **29,** 6250–6265
13. Santoro, B., Wainger, B. J., and Siegelbaum, S. A. (2004) *J. Neurosci.* **24,** 10750–10762
14. Misonou, H., and Trimmer, J. S. (2005) *J. Neurosci. Methods* **144,** 165–173
15. Lindau, M., and Neher, E. (1988) *Pflugers Arch.* **411,** 137–146
16. Zha, Q., Brewster, A. L., Richichi, C., Bender, R. A., and Baram, T. Z. (2008) *J. Neurochem.* **105,** 68–77
17. Richichi, C., Brewster, A. L., Bender, R. A., Simeone, T. A., Zha, Q., Yin, H. Z., Weiss, J. H., and Baram, T. Z. (2008) *Neurobiol. Dis.* **29,** 297–305
18. Beattie, E. C., Carroll, R. C., Yu, X., Morishita, W., Yasuda, H., von Zastrow, M., and Malenka, R. C. (2000) *Nat. Neurosci.* **3,** 1291–1300
19. El-Husseini, A. D., Schnell, E., Dakoji, S., Sweeney, N., Zhou, Q., Prange,

O., Gauthier-Campbell, C., Aguilera-Moreno, A., Nicoll, R. A., and Bredt, D. S. (2002) *Cell* **108,** 849–863
20. Brewster, A. L., Chen, Y., Bender, R. A., Yeh, A., Shigemoto, R., and Baram, T. Z. (2007) *Cereb. Cortex* **17,** 702–712
21. Vasilyev, D. V., and Barish, M. E. (2002) *J. Neurosci.* **22,** 8992–9004
22. Murphy, D. D., Cole, N. B., Greenberger, V., and Segal, M. (1998) *J. Neurosci.* **18,** 2550–2559
23. Surges, R., Brewster, A. L., Bender, R. A., Beck, H., Feuerstein, T. J., and Baram, T. Z. (2006) *Eur. J. Neurosci.* **24,** 94–104
24. Santoro, B., Chen, S., Luthi, A., Pavlidis, P., Shumyatsky, G. P., Tibbs, G. R., and Siegelbaum, S. A. (2000) *J. Neurosci.* **20,** 5264–5275
25. Santoro, B., Piskorowski, R. A., Pian, P., Hu, L., Liu, H., and Siegelbaum, S. A. (2009) *Neuron* **62,** 802–813
26. Bubb, M. R., Senderowicz, A. M., Sausville, E. A., Duncan, K. L., and Korn, E. D. (1994) *J. Biol. Chem.* **269,** 14869–14871
27. Spector, I., Braet, F., Shochet, N. R., and Bubb, M. R. (1999) *Microsc. Res. Tech.* **47,** 18–37
28. Kim, J., Jung, S. C., Clemens, A. M., Petralia, R. S., and Hoffman, D. A. (2007) *Neuron* **54,** 933–947
29. Moroni, A., Gorza, L., Beltrame, M., Gravante, B., Vaccari, T., Bianchi, M. E., Altomare, C., Longhi, R., Heurteaux, C., Vitadello, M., Malgaroli, A., and DiFrancesco, D. (2001) *J. Biol. Chem.* **276,** 29233–29241
30. Wainger, B. J., DeGennaro, M., Santoro, B., Siegelbaum, S. A., and Tibbs, G. R. (2001) *Nature* **411,** 805–810
31. Proenza, C., Tran, N., Angoli, D., Zahynacz, K., Balcar, P., and Accili, E. A. (2002) *J. Biol. Chem.* **277,** 29634–29642
32. Much, B., Wahl-Schott, C., Zong, X., Schneider, A., Baumann, L., Moosmang, S., Ludwig, A., and Biel, M. (2003) *J. Biol. Chem.* **278,** 43781–43786
33. Gravante, B., Barbuti, A., Milanesi, R., Zappi, I., Viscomi, C., and DiFrancesco, D. (2004) *J. Biol. Chem.* **279,** 43847–43853
34. Magee, J. C. (1999) *Nat. Neurosci.* **2,** 848
35. Brewster, A., Bender, R. A., Chen, Y., Dube, C., Eghbal-Ahmadi, M., and Baram, T. Z. (2002) *J. Neurosci.* **22,** 4591–4599
36. Brewster, A. L., Bernard, J. A., Gall, C. M., and Baram, T. Z. (2005) *Neurobiol. Dis.* **19,** 200–207
37. Chen, S., Wang, J., and Siegelbaum, S. A. (2001) *J. Gen. Physiol.* **117,** 491–504
38. Ulens, C., and Tytgat, J. (2001) *J. Biol. Chem.* **276,** 6069–6072
39. Zolles, G., Wenzel, D., Bildl, W., Schulte, U., Hofmann, A., Müller, C. S., Thumfart, J. O., Vlachos, A., Deller, T., Pfeifer, A., Fleischmann, B. K., Roeper, J., Fakler, B., and Klöcker, N. (2009) *Neuron* **62,** 814–825
40. Yin, H. Z., Sensi, S. L., Carriedo, S. G., and Weiss, J. H. (1999) *J. Comp. Neurol.* **409,** 250–260
41. Ogoshi, F., and Weiss, J. H. (2003) *J. Neurosci.* **23,** 10521–10530
42. de Wit, J., Toonen, R. F., Verhaagen, J., and Verhage, M. (2006) *Traffic* **7,** 1060–1077
43. de Wit, J., Toonen, R. F., and Verhage, M. (2009) *J. Neurosci.* **29,** 23–37
44. Bezzerides, V. J., Ramsey, I. S., Kotecha, S., Greka, A., and Clapham, D. E. (2004) *Nat. Cell Biol.* **6,** 709–720
45. Misonou, H., Mohapatra, D. P., Park, E. W., Leung, V., Zhen, D., Misonou, K., Anderson, A. E., and Trimmer, J. S. (2004) *Nat. Neurosci.* **7,** 711–718
46. Green, E. M., Barrett, C. F., Bultynck, G., Shamah, S. M., and Dolmetsch, R. E. (2007) *Neuron* **55,** 615–632
47. Chung, H. J., Qian, X., Ehlers, M., Jan, Y. N., and Jan, L. Y. (2009) *Proc. Natl. Acad. Sci. U.S.A.* **106,** 629–634
48. MacLean, J. N., Zhang, Y., Johnson, B. R., and Harris-Warrick, R. M. (2003) *Neuron* **37,** 109–120
49. MacLean, J. N., Zhang, Y., Goeritz, M. L., Casey, R., Oliva, R., Guckenheimer, J., and Harris-Warrick, R. M. (2005) *J. Neurophysiol.* **94,** 3601–3617
50. Meuth, S. G., Kanyshkova, T., Meuth, P., Landgraf, P., Munsch, T., Ludwig, A., Hofmann, F., Pape, H. C., and Budde, T. (2006) *J. Neurophysiol.* **96,** 1517–1529
51. Budde, T., Coulon, P., Pawlowski, M., Meuth, P., Kanyshkova, T., Japes, A., Meuth, S. G., and Pape, H. C. (2008) *Pflugers Arch.* **456,** 1061–1073